

Improving MAE against CCE under Label Noise

Xinshao Wang^{1,2}, Elyor Kodirov², Yang Hua^{1,2}, Neil M. Robertson^{1,2}

¹ School of Electronics, Electrical Engineering and Computer Science, Queen’s University Belfast, UK

² Anyvision Research Team, UK

{xwang39, y.hua, n.robertson}@qub.ac.uk, {elyor}@anyvision.co

Abstract

Label noise is inherent in many deep learning tasks when the training set becomes large. A typical approach to tackle noisy labels is using robust loss functions. Categorical cross entropy (CCE) is a successful loss function in many applications. However, CCE is also notorious for fitting samples with corrupted labels easily. In contrast, mean absolute error (MAE) is noise-tolerant theoretically, but it generally works much worse than CCE in practice. In this work, we have three main points. First, to explain why MAE generally performs much worse than CCE, we introduce a new understanding of them fundamentally by exposing their intrinsic sample weighting schemes from the perspective of every sample’s gradient magnitude with respect to logit vector. Consequently, we find that MAE’s differentiation degree over training examples is too small so that informative ones cannot contribute enough against the non-informative during training. Therefore, MAE generally underfits training data when noise rate is high. Second, based on our finding, we propose an improved MAE (IMAE), which inherits MAE’s good noise-robustness. Moreover, the differentiation degree over training data points is controllable so that IMAE addresses the underfitting problem of MAE. Third, the effectiveness of IMAE against CCE and MAE is evaluated empirically with extensive experiments, which focus on image classification under synthetic corrupted labels and video retrieval under real noisy labels.

1. Introduction

Due to the availability of large training data and powerful computation resources, deep learning has achieved great success in diverse tasks, e.g., computer vision [16], speech recognition [11], and reinforcement learning [25]. However, it becomes hard and expensive to guarantee the quality of training data as its size grows. Consequently, many deep learning tasks present inherent label confusion [4], which generally originates from many factors, such as incomplete annotation, incorrect labelling, subjectiveness, bias and so

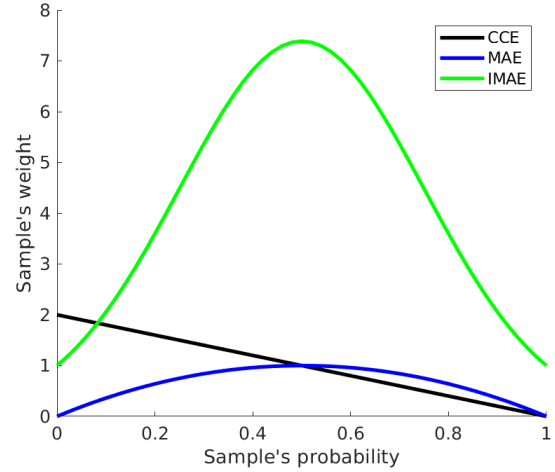


Figure 1: Sample’s weight along with probability in CCE, MAE, IMAE with $T = 8$. CCE prioritises low-probability examples where label noise probably exists. MAE and IMAE own good robustness by emphasizing on medium-probability samples. Assuming samples’ probabilities are uniformly distributed, the variances of MAE’s weighting curve and IMAE’s weighting curve are 0.09 and 4.55, respectively. Therefore, IMAE’s differentiation degree over samples is larger compared with MAE’s. Better viewed in colour.

forth. Therefore, it is significantly challenging to learn robust deep neural networks (DNNs) against overfitting to examples with noisy labels.

Great progress has been made in robustness of DNNs against corrupted labels [29, 1, 30, 9, 31, 5, 23, 14]. Some work studies robustness from regularisation perspective [29, 1], e.g., dropout [27] and data augmentation [30]. Some explores it from the angles of sample weighting [5, 23, 14] and robust loss functions [9, 31]. In this paper, instead of designing sample weighting schemes explicitly with some prior knowledge [23, 14, 5, 19], we study the robustness of DNNs from the perspective of built-in sample weighting in

loss functions. It connects sample weighting and robust loss functions together, which is inspired by the analysis of two well-known losses in [9, 31], i.e., categorical cross entropy (CCE) and mean absolute error (MAE).

According to the theoretical analysis of CCE and MAE in [9], CCE is sensitive to label noise while MAE owns robustness under label noise. In addition, [31] concludes that MAE treats training samples equally, thus being noise-robust. However, these lead to *an unanswered question*:

*Why does MAE work much worse than CCE although it is noise-robust?*¹

To answer this question, we present a better understanding of the sample weighting schemes of CCE and MAE. We understand how CCE and MAE differentiate training samples from the perspective of every sample’s gradient magnitude with respect to logit vector instead of probability vector as done in [31]. This is because the logit vector is the exact output of all parametric layers in DNNs. Consequently, we obtain a new finding: *MAE differentiates samples in a noise-robust way, but its differentiation degree over training examples is too small* as shown in Figure 1. The differentiation degree indicates the relative contribution of one example against another during training, which is determined by weight variance of all examples. Due to MAE’s small differentiation degree, informative samples cannot contribute enough against non-informative ones during training. Therefore, compared with CCE, MAE generally underfits training data when noise rate is high (Sec. 4 and 5.1.2)².

Based on our finding, we propose an improved MAE (IMAE). IMAE transforms MAE’s weighting scheme non-linearly by an exponential function, which makes the differentiation degree over training samples controllable by choosing a proper exponentiation base. On the one hand, by inheriting MAE’s overall weighting scheme, IMAE is noise-robust. On the other hand, by making the differentiation degree over training examples controllable, IMAE addresses the underfitting problem of MAE well (Sec. 4).

We present extensive empirical studies of CCE, MAE, and our IMAE on two tasks: image classification and video-based person re-identification. Regarding image classification on CIFAR-10 [15], we demonstrate the effectiveness of our IMAE against CCE and MAE consistently when the noise rate ranges from 0% to 80%. As noise rate increases, the superiority of IMAE becomes more noticeable. Moreover, it consolidates our analysis about the data fitting issues of CCE (overfitting), MAE (underfitting) and IMAE (proper fitting) in Sec. 4. In video-based person re-identification

[32] where noise exists but noise rate is unknown, and test classes are unseen during training, our IMAE also outperforms CCE, MAE significantly (Sec. 5).

2. Preliminaries

We denote an input set (a training mini-batch) as $\mathbf{X} = \{(\mathbf{x}_i, y_i)\}_{i=1}^N$, where there are N samples. (\mathbf{x}_i, y_i) represents i -th training sample $\mathbf{x}_i \in \mathbb{R}^D$ and its annotated class label $y_i \in \{1, 2, \dots, C\}$. D is the dimensionality of input samples while C is the number of classes in the entire training set instead of one specific mini-batch. Let f_θ be an embedding function, which transforms one sample \mathbf{x}_i to a feature vector $\mathbf{f}_i = f_\theta(\mathbf{x}_i) \in \mathbb{R}^E$, E is the dimensionality of feature space and θ indicates the network’s parameters to be learned. To learn deep robust feature embeddings, f_θ is a deep neural network which can be designed as different architectures (a.k.a. backbones) in different applications.

To optimise the embedding function f_θ during training, a linear classifier is generally trained jointly [7, 9, 20]. In general, the linear classifier follows the output embeddings and is composed of one C -neuron fully connected (FC) layer, one softmax normalisation layer and one loss layer. The FC layer can be represented as $\mathbf{z}_i = \mathbf{W}^\top \mathbf{f}_i \in \mathbb{R}^C$, where $\mathbf{W} = [\mathbf{w}_1, \mathbf{w}_2, \dots, \mathbf{w}_C] \in \mathbb{R}^{E \times C}$ consists of C weight vectors (the bias term is ignored for brevity). $\mathbf{z}_{ij} = \mathbf{w}_j^\top \mathbf{f}_i$ is a logit which indicates the compatibility between sample \mathbf{x}_i and class j . To produce the probabilities of sample \mathbf{x}_i belonging to different classes, we normalise every logit vector \mathbf{z}_i using a softmax function:

$$p(j|\mathbf{x}_i) = \frac{\exp(\mathbf{z}_{ij})}{\sum_{m=1}^C \exp(\mathbf{z}_{im})}, \quad (1)$$

where $p(j|\mathbf{x}_i)$ is the probability of sample \mathbf{x}_i being predicted to class j .

Let $q(j|\mathbf{x}_i)$ be the ground-truth probability of \mathbf{x}_i belonging to class j , i.e., $q(j|\mathbf{x}_i) = 1$ if $j = y_i$, $q(j|\mathbf{x}_i) = 0$ otherwise. In the loss layer, if we use CCE, the minimisation objective per iteration is:

$$\begin{aligned} L_{\text{CCE}}(\mathbf{X}; f_\theta, \mathbf{W}) &= -\frac{1}{N} \sum_{i=1}^N \sum_{j=1}^C q(j|\mathbf{x}_i) \log p(j|\mathbf{x}_i) \\ &= -\frac{1}{N} \sum_{i=1}^N \log p(y_i|\mathbf{x}_i). \end{aligned} \quad (2)$$

For MAE, the minimisation objective becomes:

$$\begin{aligned} L_{\text{MAE}}(\mathbf{X}; f_\theta, \mathbf{W}) &= \frac{1}{N} \sum_{i=1}^N \sum_{j=1}^C |p(j|\mathbf{x}_i) - q(j|\mathbf{x}_i)| \\ &= \frac{2}{N} \sum_{i=1}^N (1 - p(y_i|\mathbf{x}_i)), \end{aligned} \quad (3)$$

¹This is observed empirically in [31] and our experimental section. Therefore, MAE is much less popular than CCE in deep learning tasks.

²We analyse CCE’s overfitting and MAE’s underfitting phenomenons empirically by their classification accuracies on training sets. While fixing all other factors, the effects of different losses on fitting training data are visualised and compared.

where $|\cdot|$ is the absolute function.

As demonstrated above, when learning deep representations with the supervision of CCE or MAE, our objective is to search the optimal parameters θ and \mathbf{W} for the embedding network and linear classifier, respectively. Therefore, they can be combined together to form a deep neural network $g_{\theta, \mathbf{W}}$, which outputs logits:

$$\mathbf{z}_i = g_{\theta, \mathbf{W}}(\mathbf{x}_i) = \mathbf{W}^\top f_\theta(\mathbf{x}_i) \in \mathbb{R}^C. \quad (4)$$

In classification tasks [15, 16, 10], we use $\mathbf{z} = g_{\theta, \mathbf{W}}(\mathbf{x})$ to produce logits for a test image \mathbf{x} . While in verification or retrieval tasks, e.g., video-based person re-identification [32], we use $\mathbf{f} = f_\theta(\mathbf{x})$ as an embedding function. The overall pipeline of a deep feature embedding network is described in Figure 2.

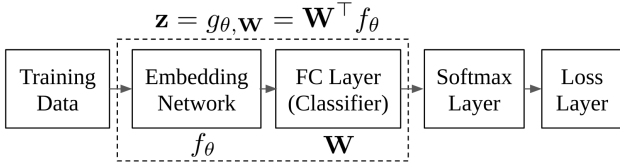


Figure 2: Pipeline of a deep feature embedding network.

3. Gradient assignment analysis

As shown in Figure 2, all parameters are contained in the embedding network and FC layer. The update of parameters θ , \mathbf{W} is based on the gradient back-propagation from logit vector \mathbf{z} . Therefore, one sample's contribution can be measured by the magnitude of its loss's derivative w.r.t. \mathbf{z} . We regard it as sample weighting that is built-in in losses.

3.1. Derivation of softmax layer

As the softmax layer is shared by CCE and MAE, we present the derivation of softmax layer first. Based on Eq. (1), we have

$$p(y_i|\mathbf{x}_i)^{-1} = 1 + \sum_{j \neq y_i} \exp(\mathbf{z}_{ij} - \mathbf{z}_{iy_i}). \quad (5)$$

If $j = y_i$, for left and right sides of Eq. (5), we calculate their derivatives w.r.t. \mathbf{z}_{iy_i} simultaneously:

$$\begin{aligned} \frac{-1}{p(y_i|\mathbf{x}_i)^2} \frac{\partial p(y_i|\mathbf{x}_i)}{\mathbf{z}_{iy_i}} &= - \sum_{j \neq y_i} \exp(\mathbf{z}_{ij} - \mathbf{z}_{iy_i}) \\ \Rightarrow \frac{\partial p(y_i|\mathbf{x}_i)}{\mathbf{z}_{iy_i}} &= p(y_i|\mathbf{x}_i)(1 - p(y_i|\mathbf{x}_i)). \end{aligned} \quad (6)$$

If $j \neq y_i$, analogously we have:

$$\begin{aligned} \frac{-1}{p(y_i|\mathbf{x}_i)^2} \frac{\partial p(y_i|\mathbf{x}_i)}{\mathbf{z}_{ij}} &= \exp(\mathbf{z}_{ij} - \mathbf{z}_{iy_i}) \\ \Rightarrow \frac{\partial p(y_i|\mathbf{x}_i)}{\mathbf{z}_{ij}} &= -p(y_i|\mathbf{x}_i)p(j|\mathbf{x}_i). \end{aligned} \quad (7)$$

In summary, the derivation of softmax layer is:

$$\frac{\partial p(y_i|\mathbf{x}_i)}{\partial \mathbf{z}_{ij}} = \begin{cases} p(y_i|\mathbf{x}_i)(1 - p(y_i|\mathbf{x}_i)), & j = y_i \\ -p(y_i|\mathbf{x}_i)p(j|\mathbf{x}_i), & j \neq y_i \end{cases} \quad (8)$$

3.2. Derivation of loss layer: CCE

According to Eq. (2), we have

$$L_{\text{CCE}}(\mathbf{x}_i; f_\theta, \mathbf{W}) = -\log p(y_i|\mathbf{x}_i). \quad (9)$$

Therefore, we obtain (the parameters are omitted for brevity),

$$\frac{\partial L_{\text{CCE}}(\mathbf{x}_i)}{\partial p(j|\mathbf{x}_i)} = \begin{cases} -p(y_i|\mathbf{x}_i)^{-1}, & j = y_i \\ 0, & j \neq y_i \end{cases}. \quad (10)$$

3.3. Derivation of loss layer: MAE

According to Eq. (3), we have

$$L_{\text{MAE}}(\mathbf{x}_i; f_\theta, \mathbf{W}) = 2(1 - (p(y_i|\mathbf{x}_i))). \quad (11)$$

Therefore, we obtain

$$\frac{\partial L_{\text{MAE}}(\mathbf{x}_i)}{\partial p(j|\mathbf{x}_i)} = \begin{cases} -2, & j = y_i \\ 0, & j \neq y_i \end{cases}. \quad (12)$$

3.4. Perspective of derivatives w.r.t. \mathbf{z}_i

It is concluded in [31] that CCE is sensitive to samples with corrupted labels while MAE treats all samples equally according to Eq. (10) and Eq. (12), respectively. On the contrary, we propose to understand the sample weighting mechanisms in CCE and MAE from the perspective of derivatives w.r.t. \mathbf{z}_i instead of $p(j|\mathbf{x}_i)$. The reason is that \mathbf{z}_i is the exact output of all parametric layers, and the update of parameters is based on the gradient back-propagation from \mathbf{z}_i . Consequently, it is interesting that we obtain different conclusions from them.

3.4.1 $\partial L_{\text{CCE}}(\mathbf{x}_i)/\partial \mathbf{z}_i$

The calculation is based on Eq. (10) and Eq. (8).

If $j = y_i$, we have:

$$\begin{aligned} \frac{\partial L_{\text{CCE}}(\mathbf{x}_i)}{\partial \mathbf{z}_{iy_i}} &= \sum_{j=1}^C \frac{\partial L_{\text{CCE}}(\mathbf{x}_i)}{\partial p(j|\mathbf{x}_i)} \frac{\partial p(y_i|\mathbf{x}_i)}{\mathbf{z}_{iy_i}} \\ &= p(y_i|\mathbf{x}_i) - 1. \end{aligned} \quad (13)$$

If $j \neq y_i$, it becomes:

$$\begin{aligned} \frac{\partial L_{\text{CCE}}(\mathbf{x}_i)}{\partial \mathbf{z}_{ij}} &= \sum_{j=1}^C \frac{\partial L_{\text{CCE}}(\mathbf{x}_i)}{\partial p(j|\mathbf{x}_i)} \frac{\partial p(y_i|\mathbf{x}_i)}{\mathbf{z}_{ij}} \\ &= p(j|\mathbf{x}_i). \end{aligned} \quad (14)$$

In summary, $\partial L_{\text{CCE}}(\mathbf{x}_i)/\partial \mathbf{z}_i$ can be represented as:

$$\frac{\partial L_{\text{CCE}}(\mathbf{x}_i)}{\partial \mathbf{z}_{ij}} = \begin{cases} p(y_i|\mathbf{x}_i) - 1, & j = y_i \\ p(j|\mathbf{x}_i), & j \neq y_i \end{cases}. \quad (15)$$

3.4.2 $\partial L_{\text{MAE}}(\mathbf{x}_i)/\partial \mathbf{z}_i$

The calculation is analogous with that of $\partial L_{\text{CCE}}(\mathbf{x}_i)/\partial \mathbf{z}_i$. According to Eq. (12) and Eq. (8), if $j = y_i$:

$$\begin{aligned} \frac{\partial L_{\text{MAE}}(\mathbf{x}_i)}{\partial \mathbf{z}_{iy_i}} &= \sum_{j=1}^C \frac{\partial L_{\text{MAE}}(\mathbf{x}_i)}{\partial p(j|\mathbf{x}_i)} \frac{\partial p(y_i|\mathbf{x}_i)}{\mathbf{z}_{iy_i}} \\ &= -2p(y_i|\mathbf{x}_i)(1 - p(y_i|\mathbf{x}_i)). \end{aligned} \quad (16)$$

otherwise ($j \neq y_i$):

$$\begin{aligned} \frac{\partial L_{\text{MAE}}(\mathbf{x}_i)}{\partial \mathbf{z}_{ij}} &= \sum_{j=1}^C \frac{\partial L_{\text{MAE}}(\mathbf{x}_i)}{\partial p(j|\mathbf{x}_i)} \frac{\partial p(y_i|\mathbf{x}_i)}{\mathbf{z}_{ij}} \\ &= 2p(y_i|\mathbf{x}_i)p(j|\mathbf{x}_i). \end{aligned} \quad (17)$$

In summary, $\partial L_{\text{MAE}}(\mathbf{x}_i)/\partial \mathbf{z}_i$ is:

$$\frac{\partial L_{\text{MAE}}(\mathbf{x}_i)}{\partial \mathbf{z}_{ij}} = \begin{cases} 2p(y_i|\mathbf{x}_i)(p(y_i|\mathbf{x}_i) - 1), & j = y_i \\ 2p(y_i|\mathbf{x}_i)p(j|\mathbf{x}_i), & j \neq y_i \end{cases}. \quad (18)$$

3.4.3 Implicit weighting in CCE and MAE

In CCE and MAE, training samples are differentiated because different samples own different gradient magnitude w.r.t. logit vector \mathbf{z} . We choose to measure one gradient's magnitude by its L_1 norm because of its simpler statistics than other norms. If one sample's gradient is larger, its contribution is larger during gradient back-propagation.

For CCE, based on Eq. (15), the weight of sample \mathbf{x}_i is:

$$w_{\text{CCE}}(\mathbf{x}_i) = \left\| \frac{\partial L_{\text{CCE}}(\mathbf{x}_i)}{\partial \mathbf{z}_i} \right\|_1 = 2(1 - p(y_i|\mathbf{x}_i)), \quad (19)$$

where $\|\cdot\|_1$ denotes L_1 norm. For MAE, based on Eq. (18), the weight of sample \mathbf{x}_i is:

$$w_{\text{MAE}}(\mathbf{x}_i) = \left\| \frac{\partial L_{\text{MAE}}(\mathbf{x}_i)}{\partial \mathbf{z}_i} \right\|_1 = 4p(y_i|\mathbf{x}_i)(1 - p(y_i|\mathbf{x}_i)). \quad (20)$$

Based on Eq. (19) and Eq. (20), both CCE and MAE differentiate samples according to their probabilities being predicted to annotated labels. The comparison between CCE and MAE is given in Sec. 4 together with our proposal, improved MAE (IMAE).

4. Improved MAE

In IMAE, we transform the original weight of MAE in Eq. (20) non-linearly:

$$w_{\text{IMAE}}(\mathbf{x}_i) = \exp(Tp(y_i|\mathbf{x}_i)(1 - p(y_i|\mathbf{x}_i))), \quad (21)$$

where T is a hyper-parameter. Specifically, the loss computation during forward propagation is unchanged. During

gradient backward propagation, we simply modify the gradient of original MAE w.r.t. logit vector as:

$$\begin{aligned} \frac{\partial L_{\text{IMAE}}(\mathbf{x}_i)}{\partial \mathbf{z}_i} &= \frac{\partial L_{\text{MAE}}(\mathbf{x}_i)}{\partial \mathbf{z}_i} \cdot \frac{w_{\text{IMAE}}(\mathbf{x}_i)}{w_{\text{MAE}}(\mathbf{x}_i)} \\ &\Rightarrow \left\| \frac{\partial L_{\text{IMAE}}(\mathbf{x}_i)}{\partial \mathbf{z}_i} \right\|_1 = w_{\text{IMAE}}(\mathbf{x}_i). \end{aligned} \quad (22)$$

Design choices. IMAE transforms the built-in weight of MAE using an exponential function, where a scaling parameter T is used to control the weighting variance, i.e., differentiation degree of training samples. Firstly, we choose exponential function because it is non-linear so that the relative weight of one sample versus another one, i.e., their relative contribution, is changed compared with original MAE. Secondly, we can choose T to differentiate samples in a proper degree under different situations. Since T is the only hyper-parameter in IMAE, it can be easily chosen on a validation set in practice. For reference, we calculate the weighting variance, i.e., the differentiation degree over training data points, of MAE and IMAE with $T = 8$ by assuming that samples' probabilities are uniformly distributed:

$$\sigma_{\text{MAE}} = \int_0^1 w_{\text{MAE}}^2(p) dp - \left(\int_0^1 w_{\text{MAE}}(p) dp \right)^2 \quad (23)$$

$$\sigma_{\text{IMAE}} = \int_0^1 w_{\text{IMAE}}^2(p) dp - \left(\int_0^1 w_{\text{IMAE}}(p) dp \right)^2. \quad (24)$$

Therefore, we have $\sigma_{\text{MAE}} = 0.09$. When $T = 8$, $\sigma_{\text{IMAE}} = 4.55$. This is also illustrated in Figure 1.

Discussion of CCE, MAE and IMAE. Figure 1 shows the curves of sample's weight along with probability in CCE, MAE and IMAE, i.e., $w_{\text{CCE}}(\mathbf{x}_i)$, $w_{\text{MAE}}(\mathbf{x}_i)$, and $w_{\text{IMAE}}(\mathbf{x}_i)$. We analyse them as follows:

- CCE prioritises samples with lower probabilities. Because corrupted samples generally own lower probabilities, they are assigned with higher weights and emphasized in CCE. Therefore, *CCE is more noise-sensitive and prone to overfitting in practice.*
- MAE assigns lower weights to both samples with high probabilities and low probabilities, thus being noise-tolerant. *MAE's weighting scheme is appealing and practical* in that samples with medium probabilities owns higher weights and are emphasized. Generally, samples with very high probabilities are trivial and non-informative. While samples with very low probabilities could be noisy as the model improves during training. Although all samples are not trained well and probabilities are not meaningful in the beginning, it

also does not hurt to focus on samples with medium probabilities. *However, the differentiation degree of training samples is too small in MAE.* Consequently, the relative contribution of one example versus another is not recognised well and a wide range of samples contribute almost equally. *Therefore, MAE generally underfits training data especially when noise rate is high.*

- IMAE inherits the noise-robustness property of MAE. Importantly, it has a hyper-parameter T that controls the differentiation degree of training samples. Empirically, when noise rate is high, we need higher differentiation degree by choosing a larger T . In practice, this T can be easily chosen using a validation set. IMAE fits training data well in our empirical studies.

These discussions are demonstrated in our empirical studies (Sec. 5.1.2). The T controls the variance of weights distribution, which reflects the differentiation degree of training examples. This is analysed in our supplementary material in more detail.

5. Experiments

In this section, we evaluate the performance of CCE, MAE, and IMAE on two tasks:

Image classification. We explore both image classification with intact labels and robust image classification where training set contains a large proportion of corrupted labels. Testing classes are joint with training classes. $\mathbf{z} = g_{\theta, \mathbf{W}}(\mathbf{x}) = \mathbf{W}^\top f_{\theta}(\mathbf{x})$ is used in the test phase.

Video-based person re-identification. It is a video retrieval problem. Given a query video, we aim to search videos of the same person from a video gallery. Testing classes are unseen during training. $\mathbf{f} = f_{\theta}(\mathbf{x})$ is used for embedding images during testing.

For IMAE, to avoid fine-tuning parameter T , we fix $T = 0.5$ on clean training sets and $T = 8$ on noisy training sets although they have different label noise rates. Because our empirical evidence suggests that it is unhelpful to differentiate samples dramatically when the training set is clean, while it helps significantly when training data contains a high proportion of noisy labels. We believe better results can be obtained by optimising T via a validation set or appealing techniques [4]³. All experiments are implemented using the Caffe [13] framework. We train the model on a Tesla V100 GPU with 32 GB RAM.

5.1. Image classification

Dataset. CIFAR-10 [15] contains 10 classes, 5k images per class for training and 1k images per class for testing. The image size is 32×32 .

³More discussion about weighting hyper-parameter T is given in the supplementary material.

Table 1: Classification accuracy of CCE, MAE, and IMAE on CIFAR-10. Backbone architectures with different depth are explored.

Dataset	Model	CCE	MAE	IMAE
CIFAR-10	ResNet20	91.0	89.9	91.4
	ResNet32	92.5	82.4	92.1
	ResNet56	92.5	89.0	92.7

Implementation details⁴. We follow the study on CIFAR-10 in [10], which means we use exactly same architectures (ResNet20, ResNet32, ResNet56) and training settings: a weight decay of 0.0001, a momentum of 0.9, a batch size of 128. The learning rate starts at 0.1, then is divided by 10 at 32k and 48k iterations. Training stops at 64k iterations. We use the same data augmentation techniques: random horizontal flips and crops of 32×32 on the original images padded with 4 pixels on each side.

5.1.1 CIFAR-10 with intact labels

In Table 1, we compare our IMAE against CCE and MAE on CIFAR-10 with different nets (ResNet20, ResNet32, ResNet56). From shallower to deeper architectures, we observe that: (1) IMAE is highly competitive with CCE consistently; (2) IMAE outperforms MAE significantly.

5.1.2 CIFAR-10 with corrupted labels

Motivated by recent work [29, 1, 30], we evaluate the robustness of deep models against corrupted labels. The memorisation of noisy labels has been studied from the perspective of regularisation [29, 1] and data augmentation [30]. In this work, we present an analysis of it from the perspective of sample weighting in loss functions. Interestingly, we alleviate both overfitting and underfitting by weighting training samples properly.

Corrupted training sets. We corrupt CIFAR-10 training labels following [29, 30]. With a probability r , the label of each image is replaced by a random integer from 0 to 9. Since the new label is chosen at random, it may be identical to the original one. Therefore, the noise rate is around r . All training instances generated from an original image by data augmentation share the same label. As in [29, 30], we choose three different noise rates to compare the deep models supervised by different losses, i.e., $r = 20\%$, 50% , and 80% . Note that all test labels are kept intact.

Results. In the context of different noise rates, different losses with two architectures of different depth (ResNet20 and ResNet32) are studied. The results are summarised in Table 2. The accuracy on corrupted training sets along with

⁴Our focus is to study and compare the behaviours of CCE, MAE and IMAE instead of pushing the state-of-the-art on CIFAR-10.

Table 2: Results of CCE, MAE, IMAE on CIFAR-10 with corrupted labels. For classification accuracy on the test set, we show the best result achieved during training and the final result when training stops, which are indicated by ‘Best’ and ‘Final’, respectively. For training accuracy, the results on corrupted training sets and original intact set are presented. Since the overlap rate between corrupted and intact sets is $(1 - r)$, the accuracy on intact training set is only for reference.

Backbone	Label corruption	Loss	Test accuracy		Training accuracy	
			Best	Final	Corrupted	Intact
ResNet20	20%	CCE	87.1	83.2	85.1	90.6
		MAE	87.8	87.8	78.2	93.0
		IMAE	88.0	84.6	76.6	90.2
	50%	CCE	79.7	69.5	62.4	74.0
		MAE	75.6	75.3	48.8	79.0
		IMAE	83.0	80.9	56.8	85.6
	80%	CCE	56.1	38.5	42.0	40.9
		MAE	45.3	45.1	20.3	46.1
		IMAE	71.5	62.8	34.9	65.3
ResNet32	20%	CCE	87.6	81.2	85.5	88.3
		MAE	80.6	80.4	71.7	85.0
		IMAE	87.8	85.3	77.7	91.2
	50%	CCE	79.9	62.8	71.2	66.7
		MAE	61.6	61.6	40.3	64.0
		IMAE	84.1	80.4	57.9	84.7
	80%	CCE	57.6	32.7	50.9	35.1
		MAE	43.8	43.7	19.1	44.3
		IMAE	71.0	68.7	31.9	71.2

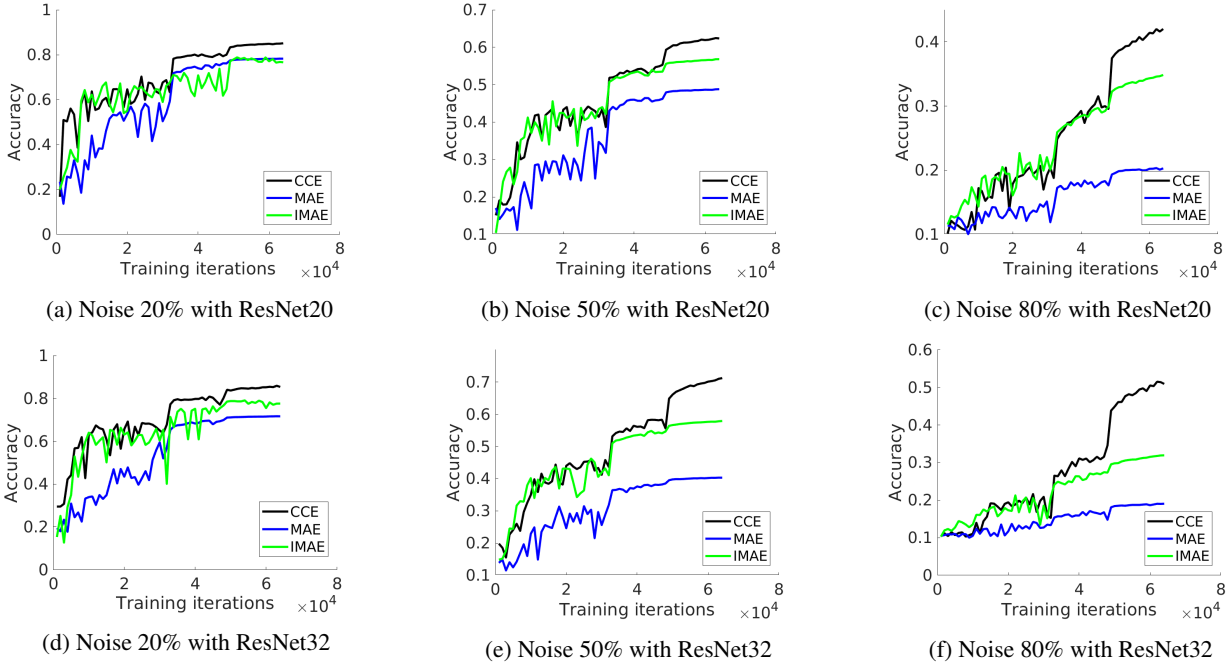


Figure 3: The accuracy on CIFAR-10 corrupted training sets (Noise 20%, 50%, 80%) along with training iterations. The results of ResNet20 and ResNet32 are presented. *Better viewed in colour.*

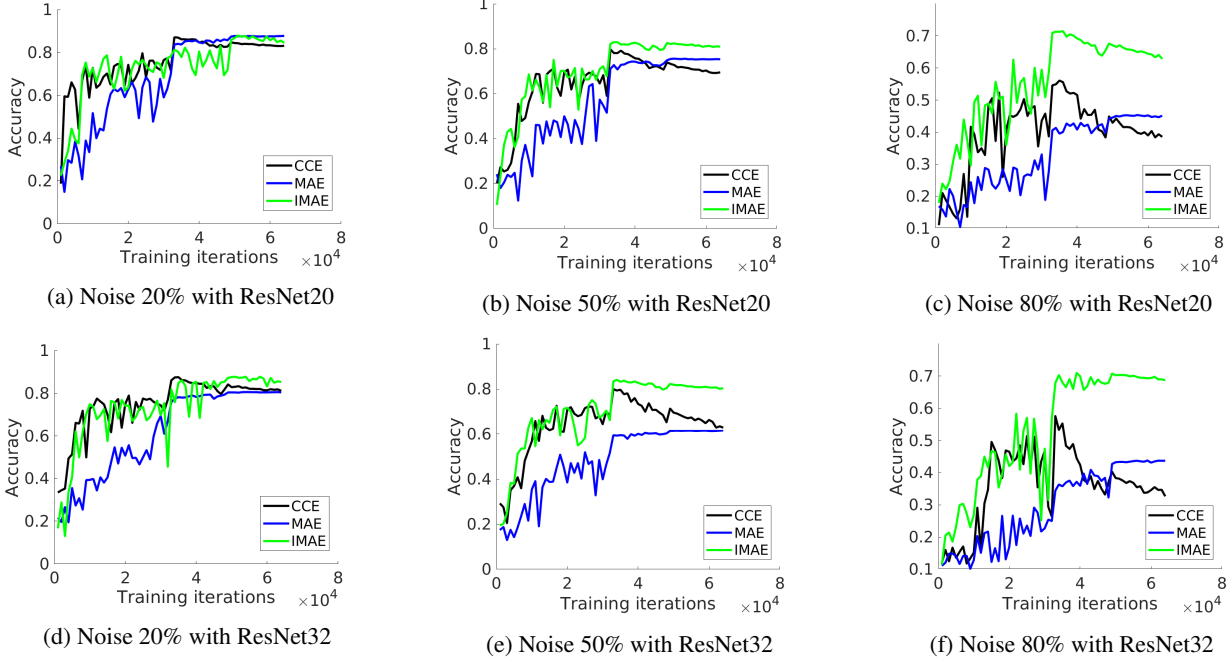


Figure 4: The accuracy on CIFAR-10 test set along with training iterations. Training labels are corrupted with different noise rate. The results of ResNet20 and ResNet32 are presented. *Better viewed in colour.*

training iterations is shown in Figure 3. The accuracy on intact test set along with training iterations is shown in Figure 4. We have the following observations:

- Regarding CCE’s test accuracies, the best one is always much higher than the final one according to Table 2 and Figure 4. When fixing the architecture, their gap becomes larger as the noise rate r increases from 20% to 80%. While fixing the noise rate, the gap also becomes more dramatic when network is deeper. We can understand the reason from Figure 3. *As training goes, CCE always tries to fit training data better.* Therefore, when the noise rate is high and the model’s fitting ability is strong with deep networks, CCE leads to overfitting easily.
- Looking at test accuracies of MAE and IMAE, the gap between the best and final accuracies is significantly smaller than that of CCE regardless of noise rate and network depth. Especially, MAE’s final accuracy is almost the same as the best accuracy. Therefore, MAE and IMAE is much more noise-robust than CCE.
- In terms of fitting training data, the accuracies on corrupted training set in Table 2 and Figure 3 are informative. Independent of noise rate and network depth, CCE fits the corrupted set much better than MAE and IMAE. Moreover, CCE always tries to fit it better as training goes. That is why overfitting occurs and its testing accuracy drops gradually in Figure 4. When it

comes to MAE, except for $r = 20\%$ with ResNet20, both training and test accuracies are much lower than those of CCE and IMAE. We observe that MAE underfits training data in majority cases in Figure 3.

These observations are consistent with our fundamental analysis in Sec. 4. *CCE overfits training data easily* because it always emphasises on samples that are not trained well and tries to fit them. However, CCE also fits noisy samples which are usually assigned with high weights, thus leading to bad generalisation performance. *MAE generally underfits training set* especially when noise rate is high. MAE does not have large enough differentiation degree on training samples. As a result, informative samples cannot contribute enough against non-informative ones. Therefore, MAE converges to a bad local optima easily. *IMAE inherits noise-robustness from MAE and addresses MAE’s underfitting issue well.* On noisy training sets, we fix $T = 8$ so that IMAE has large enough differentiation degree of samples so that informative training instances can contribute enough.

5.2. Video-based person re-identification

Dataset and evaluation protocol. MARS [32] is one of the largest benchmarks. It contains 20,715 videos of 1,261 persons. There are 1,067,516 person frames in total. The image size is 128×64 . Because person tracklets and frames are collected automatically by tracking and detection algorithms [6, 8], a lot of images contain a different person or only background [28]. Following the evaluation setting ex-

actly [32], we use 8,298 videos of 625 persons for training (509,914 images in total) and 12,180 tracklets of 636 persons for testing (681,089 images in total). We report the Cumulated Matching Characteristics (CMC) and mean average precision (mAP) performance.

Implementation details.⁵ Following [21, 28], we choose GoogleNet with batch normalisation [12] as the backbone network. We also follow them to treat each video as an image set so that we use only images’ appearance information without exploiting the temporal information. A tracklet’s representation is simply the average fusion of images’ representations in the tracklet. *The training settings are the same for each method.* The learning rate starts from 0.01 and is divided by 2 every 10k iterations. We stop training at 50k iterations. We choose SGD optimiser with a weight decay of 0.0005 and momentum of 0.9. The batch size is set to 180. We use simple data augmentation for training: a 224×224 crop is randomly sampled and flipped after resizing the original image to 256×256 . Following [21, 28, 26, 22, 18], we first L_2 normalise tracklets’ features and then calculate the cosine similarity between every two features. The final model when training stops is used for testing.

Results. We compare our method with CCE, MAE and [31]⁶. In this case, note that we do not corrupt any labels, thus the exact noise rate is unknown. The results are shown in Table 3. We find that IMAE outperforms all methods by a significant margin, verifying our analysis in Sec. 5.1.2.

Table 3: The experimental results of CCE, MAE, [31] and IMAE on MARS in terms of mAP (%) and CMC-1 (%).

Metric	CCE	MAE	[31]	IMAE
mAP (%)	58.1	12.0	31.6	70.9
CMC-1 (%)	73.8	26.0	51.5	83.5

6. Related work

There is a lot of work on increasing DNNs’ robustness against overfitting to corrupted labels [29, 1, 30]. In this work, IMAE is proposed to learn a robust model that fits training data well by analysing intrinsic sample weighting schemes of CCE and MAE. Therefore, our work is closely related to some work about sample weighting [23, 14, 5, 19] and robust loss functions [9, 31].

Sample weighting. In Examples Reweighting [23], a meta-learning algorithm learns to assign weights to training examples according to their gradient directions. The

meta-learning algorithm is optimised on a clean validation set. In contrast, our IMAE assigns weights to samples based on their gradient magnitude and does not require extra clean set. MentorNet [14] learns data-driven sample weighting scheme, which guides StudentNet to focus on samples whose labels are more likely to be correct. Instead of training an extra network like MentorNet [14], we focus on the loss function, which is easier in practice. In Active Bias [5] and Focal Loss [19], uncertain and hard examples are emphasized, respectively. Therefore, their weighting schemes are considerably different. Other related work on weighting samples includes curriculum learning [3], self-paced learning [17], and hard examples mining [24, 28]. *In summary, what makes ours different is that the weighting scheme of IMAE inherits from MAE and comes from the angle of gradient magnitude.* It is built-in in the loss function.

Robust loss functions. [9, 31] are closely related to our work. They analyse the robustness of losses from the perspective of symmetry condition, i.e, the boundness of loss values. Besides, [31] provides an analysis on the gradient w.r.t. probabilities, and proposes a generalised framework to achieve a balance between CCE and MAE. However, [31] requires data pruning and alternative convex search [2], making it complex in practice. Contrary to them, we present an analysis about the gradient w.r.t. logit vector, whose magnitude indicates the weight/contribution of an example. Interestingly, it leads to new conclusions, which motivate us to propose IMAE, a much simpler solution.

7. Conclusion

In this work, we analyse and address data fitting issue in DNNs from the angle of built-in sample weighting in loss functions. We present a fundamental analysis that CCE inherently focuses on low-probability examples while MAE prioritises medium-probability ones. However, MAE’s differentiation degree of samples is too small, leading to informative ones cannot contribute enough against non-informative ones. Consequently, CCE easily overfits training data while MAE generally underfits it. Therefore, we propose IMAE, which inherits noise-robustness from MAE and addresses its underfitting issue well. Apart from being fundamental, extensive experiments demonstrate IMAE’s effectiveness and robustness. We conclude that differentiating training samples properly is a key to learning a robust model.

References

- [1] D. Arpit, S. Jastrzebski, N. Ballas, D. Krueger, E. Bengio, M. S. Kanwal, T. Maharaj, A. Fischer, A. Courville, Y. Bengio, and S. Lacoste-Julien. A closer look at memorization in deep networks. In *ICML*, 2017. 1, 5, 8

⁵Our focus is to explore the performance of different losses in real-world applications instead of pushing the state-of-the-art results.

⁶[31] is a generalised version of cross-entropy which is robust to noise. We implement the loss function with their best setting proposed in [31].

- [2] M. S. Bazaraa, H. D. Sherali, and C. M. Shetty. *Nonlinear programming: theory and algorithms*. John Wiley & Sons, 2013. 8
- [3] Y. Bengio, J. Louradour, R. Collobert, and J. Weston. Curriculum learning. In *ICML*, 2009. 8
- [4] L. Berrada, A. Zisserman, and M. Pawan Kumar. Smooth loss functions for deep top-k classification. *ICLR*, 2018. 1, 5
- [5] H.-S. Chang, E. Learned-Miller, and A. McCallum. Active bias: Training more accurate neural networks by emphasizing high variance samples. In *NIPS*, 2017. 1, 8
- [6] A. Dehghan, S. Modiri Assari, and M. Shah. Gmmcp tracker: Globally optimal generalized maximum multi clique problem for multiple object tracking. In *CVPR*, 2015. 7
- [7] G. Elsayed, D. Krishnan, H. Mobahi, K. Regan, and S. Bengio. Large margin deep networks for classification. In *NIPS*, 2018. 2
- [8] P. F. Felzenszwalb, R. B. Girshick, D. McAllester, and D. Ramanan. Object detection with discriminatively trained part-based models. *IEEE Transactions on Pattern Analysis and Machine Intelligence*, 2010. 7
- [9] A. Ghosh, H. Kumar, and P. Sastry. Robust loss functions under label noise for deep neural networks. In *AAAI*, 2017. 1, 2, 8
- [10] K. He, X. Zhang, S. Ren, and J. Sun. Deep residual learning for image recognition. In *CVPR*, 2016. 3, 5
- [11] G. Hinton, L. Deng, D. Yu, G. Dahl, A.-r. Mohamed, N. Jaitly, A. Senior, V. Vanhoucke, P. Nguyen, B. Kingsbury, et al. Deep neural networks for acoustic modeling in speech recognition. *IEEE Signal processing magazine*, 29, 2012. 1
- [12] S. Ioffe and C. Szegedy. Batch normalization: Accelerating deep network training by reducing internal covariate shift. In *ICML*, 2015. 8
- [13] Y. Jia, E. Shelhamer, J. Donahue, S. Karayev, J. Long, R. Girshick, S. Guadarrama, and T. Darrell. Caffe: Convolutional architecture for fast feature embedding. In *ACMMM*, 2014. 5
- [14] L. Jiang, Z. Zhou, T. Leung, L.-J. Li, and L. Fei-Fei. Mentornet: Learning data-driven curriculum for very deep neural networks on corrupted labels. In *ICML*, 2018. 1, 8
- [15] A. Krizhevsky. Learning multiple layers of features from tiny images. 2009. 2, 3, 5
- [16] A. Krizhevsky, I. Sutskever, and G. E. Hinton. Imagenet classification with deep convolutional neural networks. In *NIPS*, 2012. 1, 3
- [17] M. P. Kumar, B. Packer, and D. Koller. Self-paced learning for latent variable models. In *NIPS*, 2010. 8
- [18] M. T. Law, R. Urtasun, and R. S. Zemel. Deep spectral clustering learning. In *ICML*, 2017. 8
- [19] T.-Y. Lin, P. Goyal, R. Girshick, K. He, and P. Dollar. Focal loss for dense object detection. In *ICCV*, 2017. 1, 8
- [20] W. Liu, Y. Wen, Z. Yu, and M. Yang. Large-margin softmax loss for convolutional neural networks. In *ICML*, 2016. 2
- [21] Y. Liu, J. Yan, and W. Ouyang. Quality aware network for set to set recognition. In *CVPR*, 2017. 8
- [22] Y. Movshovitz-Attias, A. Toshev, T. K. Leung, S. Ioffe, and S. Singh. No fuss distance metric learning using proxies. In *ICCV*, 2017. 8
- [23] M. Ren, W. Zeng, B. Yang, and R. Urtasun. Learning to reweight examples for robust deep learning. In *ICML*, 2018. 1, 8
- [24] A. Shrivastava, A. Gupta, and R. Girshick. Training region-based object detectors with online hard example mining. In *CVPR*, 2016. 8
- [25] D. Silver, A. Huang, C. J. Maddison, A. Guez, L. Sifre, G. Van Den Driessche, J. Schrittwieser, I. Antonoglou, V. Panneershelvam, M. Lanctot, et al. Mastering the game of go with deep neural networks and tree search. *Nature*, page 484, 2016. 1
- [26] H. O. Song, S. Jegelka, V. Rathod, and K. Murphy. Deep metric learning via facility location. In *CVPR*, 2017. 8
- [27] N. Srivastava, G. Hinton, A. Krizhevsky, I. Sutskever, and R. Salakhutdinov. Dropout: a simple way to prevent neural networks from overfitting. *The Journal of Machine Learning Research*, pages 1929–1958, 2014. 1
- [28] X. Wang, Y. Hua, E. Kodirov, G. Hu, and N. M. Robertson. Deep metric learning by online soft mining and class-aware attention. In *AAAI*, 2019. 7, 8
- [29] C. Zhang, S. Bengio, M. Hardt, B. Recht, and O. Vinyals. Understanding deep learning requires rethinking generalization. In *ICLR*, 2017. 1, 5, 8
- [30] H. Zhang, M. Cisse, Y. N. Dauphin, and D. Lopez-Paz. mixup: Beyond empirical risk minimization. *ICLR*, 2018. 1, 5, 8
- [31] Z. Zhang and M. R. Sabuncu. Generalized cross entropy loss for training deep neural networks with noisy labels. 2018. 1, 2, 3, 8
- [32] L. Zheng, Z. Bie, Y. Sun, J. Wang, C. Su, S. Wang, and Q. Tian. Mars: A video benchmark for large-scale person re-identification. In *ECCV*, 2016. 2, 3, 7, 8

Supplementary Material

1. The impact of T on differentiation degree

The differentiation degree over training samples is indicated by the weighting variance. It reflects the relative contribution of one example versus another during training. We show the weighting curves of IMAE with different T in Figure 5.

Assuming samples' probabilities are uniformly distributed, we calculate the variances of IMAE's weighting curves with different T . As illustrated in Sec. 4 of the main paper, we rewrite the Eq. (21) (We use e to replace \exp for brevity):

$$w_{\text{IMAE}}(p) = e^{Tp(1-p)}, \quad (25)$$

where p is the probability of one randomly sampled example being predicted to its annotated label. According to Eq. (24) in the main paper, we have,

$$\begin{aligned} \sigma_{\text{IMAE}} &= \int_0^1 w_{\text{IMAE}}^2(p) dp - \left(\int_0^1 w_{\text{IMAE}}(p) dp \right)^2 \\ &= \int_0^1 e^{2Tp(1-p)} dp - \left(\int_0^1 e^{Tp(1-p)} dp \right)^2 \\ &= \frac{\sqrt{\pi} \operatorname{erf}\left(\frac{\sqrt{2T}}{2}\right) e^{\frac{T}{2}}}{\sqrt{2T}} - \frac{\pi \operatorname{erf}^2\left(\frac{\sqrt{T}}{2}\right) e^{\frac{T}{2}}}{T}. \end{aligned} \quad (26)$$

erf is the error function. Therefore we obtain the weighting variances σ_{IMAE} of IMAE with different T , as displayed in Table 4. In the main paper, in cases where corrupted training labels exist, we simply fix $T = 8$ (IMAE-8) without any tuning.

Table 4: The weighting variances (differentiation degree over training data points) of IMAE with different T .

T	16	8	4	2	1	0.5	0
σ_{IMAE}	354.113	4.546	0.299	0.040	0.007	0.002	0

2. The impact of T on test accuracy

We visualise and compare the effect of T on CIFAR-10 test performance. These experiments follow exactly the

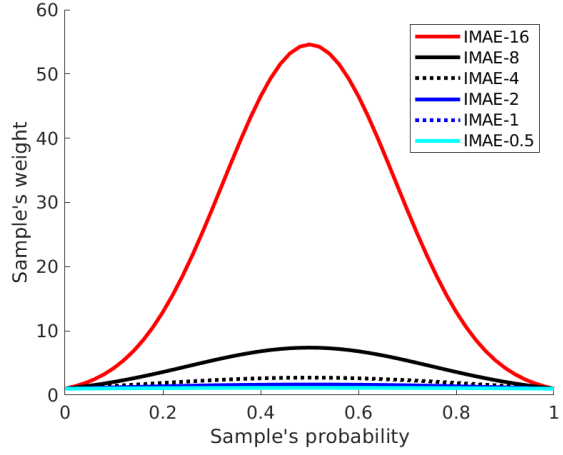


Figure 5: Sample's weight along with probability in IMAE with different T (IMAE- T). The hyper-parameter T controls weighting variance, i.e., differentiation degree over training data points. *Better viewed in colour.*

same settings of the main paper. We choose different T in different experiments.

We try two cases: (1). Training labels are intact ($r = 0$); (2). Training labels are corrupted randomly with a label noise rate of 50% ($r = 50\%$). In both cases, the test set is kept intact for evaluation. The backbone network is ResNet20.

2.1. CIFAR-10 with intact training labels

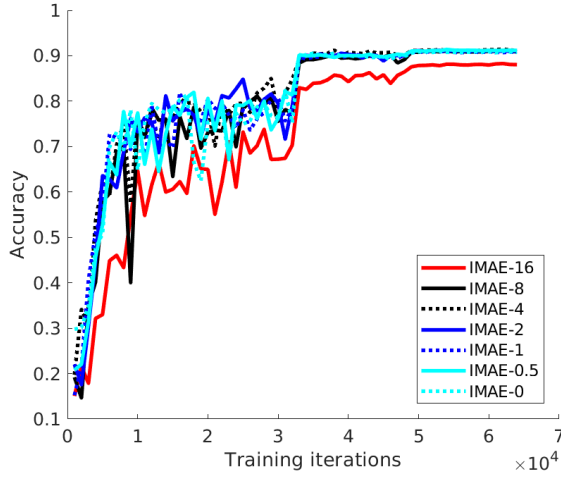
The test results are shown and compared in Figure 6a.

When training labels are clean, it is unhelpful to differentiate training samples in a high degree, e.g., the performance is even lower when $T = 16$. The final test accuracies are similar when T ranges from 0 to 8.

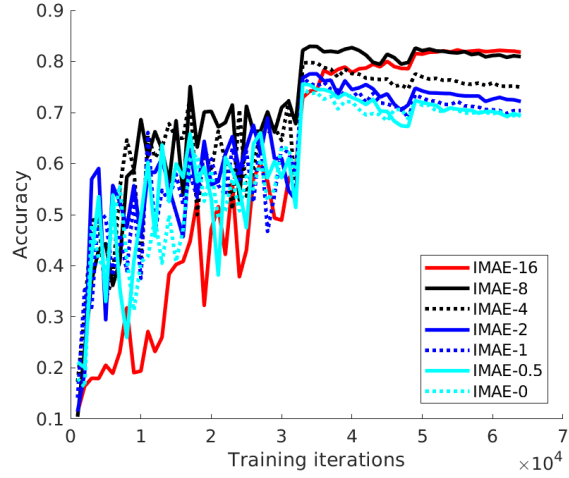
2.2. CIFAR-10 with corrupted training labels

The results are presented and compared in Figure 6b.

Because there exists 50% label noise, as training goes, the test accuracy drops, which means the model overfits noisy data gradually. However, we observe that higher differentiation degree (larger T) works better and is much less brittle to overfitting to noisy data. In Figure 6b, the final

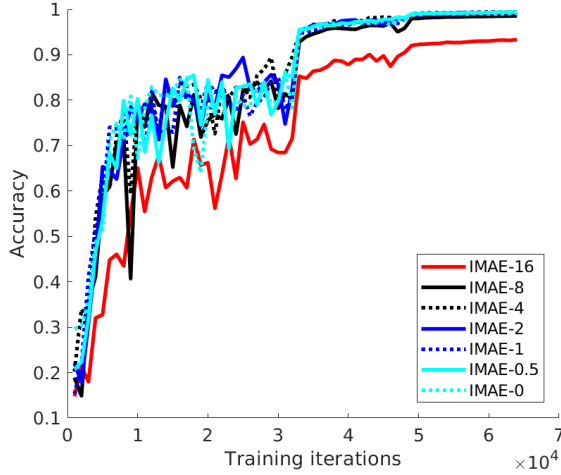


(a) The test accuracies of IMAE- T with intact training labels.

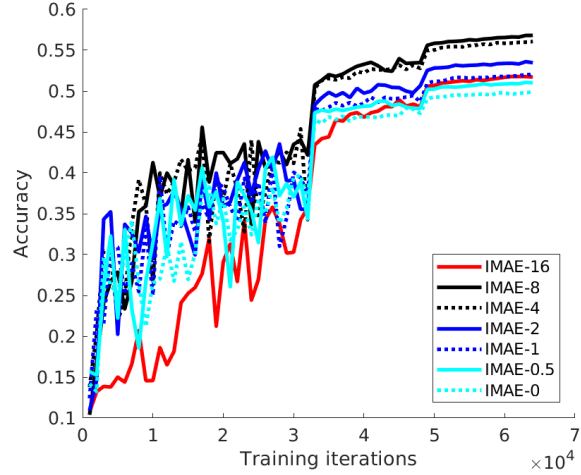


(b) The test accuracies of IMAE- T with corrupted training labels.

Figure 6: The accuracy on CIFAR-10 *test set* along with training iterations. We study and compare intact training set ($r = 0$) and corrupted training set ($r = 50\%$). *Better viewed in colour.*



(a) The training accuracies of IMAE- T on intact training set.



(b) The training accuracies of IMAE- T on corrupted training set.

Figure 7: The accuracy on CIFAR-10 *training sets* along with training iterations. We study and compare intact training set ($r = 0$) and corrupted training set ($r = 50\%$). *Better viewed in colour.*

test accuracies of IMAE-16 and IMAE-8 is much higher than those of other models.

3. The impact of T on training accuracy

Following the practice in the main paper, we also visualise and compare the accuracies on the training sets, which indicate how different models fit to training data as training goes, thus leading to different generalisation performance in the test phase. All models are trained in experiments of Sec. 2. We present how each model fits its corresponding training set in Figure 7.

3.1. Fitting of intact training set

As compared in Figure 7a, all models fit training data similarly when T ranges from 0 to 8. However, when $T = 16$, the differentiation degree becomes too large as shown in Table 4. *When differentiation degree is too large, only a quite small proportion of training data can contribute.* Consequently, IMAE-16 underfits training data compared with other models. That is why IMAE-16 has the worst test performance as shown in Figure 6a.

3.2. Fitting of corrupted training set

The training accuracies of corrupted training set are displayed in Figure 7b. We have two observations:

- In cases where noise rate is high, as T increases, the fitting of training data first becomes better, and then becomes worse. Specifically, when T increases from 0 to 8, the training accuracy grows gradually, which means the fitting of training data becomes better. However, when $T = 16$, the weighting variance becomes very large (Table 4). As a result, IMAE-16's fitting of training data becomes much worse than IMAE-8's.
- Fitting corrupted training data better does not mean better generalisation performance. On the one hand, although IMAE-16 fits the training data much worse than IMAE-8 (Figure 7b), IMAE-16's test accuracy is slightly better than IMAE-8's (Figure 6b). On the other hand, similar to IMAE-8, IMAE-4 fits its training data well (Figure 7b), but IMAE-4's test performance is much worse than IMAE-8's (Figure 6b).

4. Choosing T in practice

In summary, the training accuracy (fitting of training data) is uninformative for estimating a model's generalisation performance according to our findings in Section 3.2. Therefore, it is better to optimise T on a validation set in practice.

For empirical demonstration, since the overlap rate between corrupted and intact training sets is only $(1 - r) = 50\%$, we treat the original intact training set as a validation set. The validation performance of IMAE-16, IMAE-8 and IMAE-4 is compared in Figure 8. We observe that IMAE-

16 and IMAE-8 own similar validation performance, while IMAE-4's validation accuracy is lower. Furthermore, their validation performance is consistent with their test performance (Figure 6b).

Therefore, we conclude that it is a good practice to optimise T on a validation set in different cases. Similar evidences can be observed in Table 2 of the main paper, where IMAE's accuracies on the intact training set (validation set) are much higher than CCE's and MAE's except for $r = 20\%$ with ResNet20.

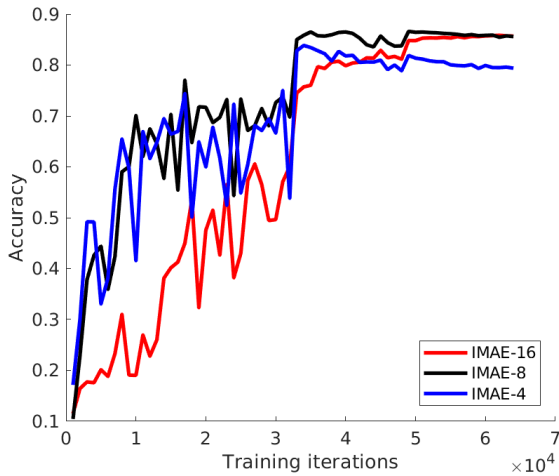


Figure 8: IMAE-16's, IMAE-8's and IMAE-4's accuracies on the original intact training set when they are trained on the corrupted training set ($r = 50\%$). The overlap rate between corrupted and intact training sets is only $(1 - r) = 50\%$. Therefore, we can use the original training set as a validation set. Better viewed in colour.